Precise modeling of the B_s^0 meson invariant mass distribution in the $B_s^0 \to J/\psi(\mu^+\mu^-)\phi(K^+K^-)$ channel using data from the ATLAS experiment at the LHC

Honors Thesis: Luis V. Flores Sanchez

Advisors: Radek Novotny & Sally Seidel

University of New Mexico

Date: May 2025

Abstract

A model of the B_s^0 meson mass has been developed using data from decays in the channel $B_s^0 \to J/\psi(\mu^+\mu^-)\phi(K^+K^-)$ based on information from the ATLAS experiment at the LHC. The data were collected during LHC Runs 2 and 3. This analysis contributes to the measurement of the $B_s^0 \to J/\psi(\mu^+\mu^-)\phi(K^+K^-)$ decay branching ratio which probes CP violation due to interference between a direct decay and a decay with $B_s^0 - \overline{B_s^0}$ mixing. Precise fits of peaking and combinatorial backgrounds are applied. Assessment of the stability of the reconstructed mass as a function of transverse momentum and over time is carried out as it is an essential contribution to the understanding of the systematic error of the measurement of the branching ratio.

Acknowledgments

I would like to express my immense gratitude to Radek Novotny & Sally Seidel for their invaluable assistance and support throughout the duration of this research. I would also like to thank Maria Smizanska of Lancaster University and the rest of the high-energy physics team at the University of New Mexico for their assistance.

Contents

List of Figures

Chapter 1

Overview

In this paper the $B_s^0 \to J/\psi\phi$ mass distribution is modeled using a variety of functions. This aims to improve fitting parameters in the previous $B_s^0 \to J/\psi\phi$ analysis [1]. This research focuses on analyzing variations in mass distributions across different LHC Run 2 datasets and specific transverse momentum (p_T) regions. The extraction of mass distribution parameters is necessary for the characterization of the $B_s^0 - \bar{B}_s^0$ CP-violating phase ϕ_s.

To achieve this, Monte Carlo [2] simulations based on ATLAS Run 2 data from 2015 and 2016 were used to predict signal and background contributions to the $B_s^0 \to J/\psi\phi$ decay. The B_s^0 background contributions include the $B_d^0 \to J/\psi K^{0*}$ background.

Figure 1.1 shows a previous ATLAS analysis which modeled the $B_s^0 \to J/\psi\phi$ distribution using Gaussians and exponential functions [1]. The analysis used data from the years 2015 to 2017.

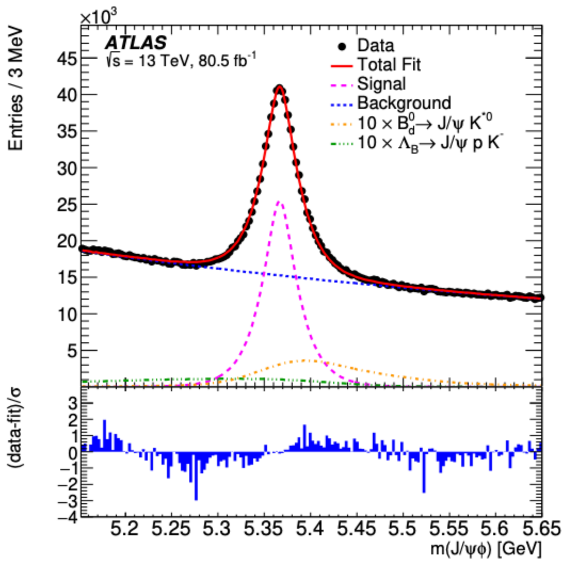

Figure 1.1: $B_s^0 \to J/\psi\phi$ model from an earlier ATLAS analysis [1].

Chapter 2

Introduction

The Standard Model of Particle Physics (SM) [3] is a theory that describes the constituent particles within our universe. It is the most successful theory in particle physics. It includes 12 fundamental *fermions* and their 12 antiparticles. There exist 4 types of *gauge bosons* that govern interactions between the 12 fermions. The Standard Model unifies 3 of the 4 fundamental forces of nature: the weak force, strong force and electromagnetic force. This can be seen Figure 2.1.

2.1 Deficiencies of the Standard Model

Although the SM is an extremely successful theory, it does not explain the existence of dark matter nor dark energy in the universe. According to various calculations, only about 5% of our universe is normal matter, while 27% is dark matter and 68% is dark energy [4]. This sparks our exploration for physics beyond the Standard Model to attempt to explain such discrepancies.

The SM also fails to explain why there is abundantly more matter than antimatter [5]. This is important for the context of the paper ahead.

2.2 Charge parity violation

Conservation of the product, charge conjugation times parity (CP), implies that the laws of physics should be the same if a particle is interchanged with its antiparticle (charge conjugated) while its spatial coordinates are inverted (parity symmetry). In certain neutral mesons such as the B_s^0 and B_d^0, different rates occur for CP conjugates [6]. This violates CP conservation.

The Cabibbo-Kobayashi-Maskawa (CKM) matrix contains information on the amplitudes for the flavor-changing weak interaction. It relates states according to Eq. (2.1),

$$\begin{bmatrix} d' \\ s' \\ b' \end{bmatrix} = \begin{bmatrix} V_{ud} & V_{us} & V_{ub} \\ V_{cd} & V_{cs} & V_{cb} \\ V_{td} & V_{ts} & V_{tb} \end{bmatrix} \begin{bmatrix} d \\ s \\ b \end{bmatrix} . \tag{2.1}$$

Here,

- the left-hand column includes the weak interaction eigenstates,
- V_{ij} represents the amplitude for a transition from a quark of flavor *i* to one of flavor *j*,
- and the right column indicates the mass eigenstates of the particles.

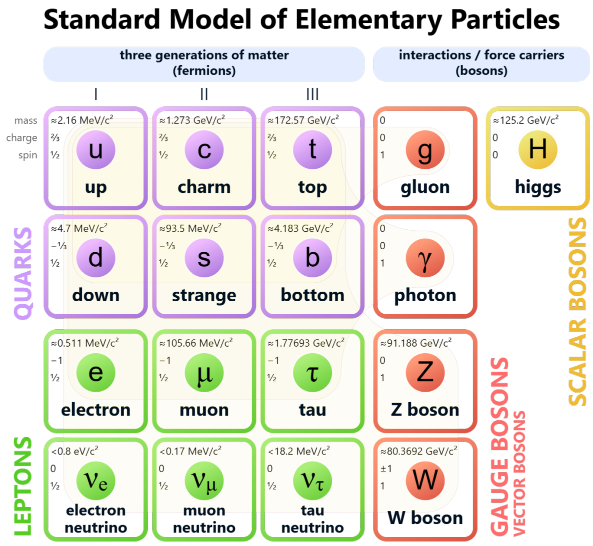

Figure 2.1: The particles included in the Standard Model of Particle Physics [3].

The standard representation of the CKM matrix is shown in Eq. (2.2),

$$V_{CKM} = \begin{pmatrix} c_{12} & s_{12}c_{13} & s_{13}e^{-i\delta_{13}} \\ -s_{12}c_{23} - c_{12}s_{23}s_{13}e^{i\delta_{13}} & c_{12}c_{23} - s_{12}s_{23}s_{13}e^{i\delta_{13}} & s_{23}c_{13} \\ s_{12}s_{23} - c_{12}c_{23}s_{13}e^{i\delta_{13}} & -c_{12}s_{23} - s_{12}c_{23}s_{13}e^{i\delta_{13}} & c_{23}c_{13} \end{pmatrix}, \tag{2.2}$$

where θ_{ij} represents the amplitude for each flavor-changing interaction under weak interactions and the cosines and sines of the angles θ_{ij} are denoted as c_{ij} and s_{ij} for *i*,*j* = [1, 2, 3] respectively. The CKM matrix contains one complex phase element δ_{13}. The δ_{13} describes the CP-violating phase in the CKM matrix. It affects processes where the interference between different decay amplitudes is directly observable as in the $B_s^0 \to J/\psi\phi$ decay channel.

Characterizing this phase difference may give insights into the matter-antimatter asymmetry and New Physics. This is because one of the contributors to the imbalance of matter and antimatter is CP violation, as stated in the Sakharov conditions [7].

2.3 The LHC and the ATLAS Detector

The Large Hadron Collider (LHC) is the world's largest particle accelerator, situated up to 175m underground at CERN near Geneva, Switzerland. The ring is designed to accelerate hadrons, primarily protons but also heavy ions, at speeds close to the speed of light. The LHC collides particles at 4 main interaction points along the ring; this is where the LHC hosts its four main detectors – ATLAS, CMS, LHCb and ALICE. The ATLAS detector is a multipurpose detector designed to detect the broadest range of signals that New Physics processes might provide [8]. ATLAS records 600 million collisions per second. The data for this analysis were taken using the ATLAS detector.

When a collision occurs at LHC Point 1, outgoing particles traverse the ATLAS detector. These particles generate signals in the inner trackers, calorimeters, and muon spectrometer. To deal with the large flux of events, the trigger system selects relevant collisions by applying kinematic cuts on the incoming data. This process allows ATLAS to collect data that are of interest. Offline reconstruction algorithms reconstruct particle tracks using the Inner Detector and determine which tracks are likely to have emerged from common vertices. Specialized components within the ATLAS detector aid in the identification of the particles produced in the collision. The Inner Detector tracks charged particles, the calorimeters measure the energy of electrons and hadrons, the muon spectrometer identifies muons based on their penetration depth through the detector and the magnetic field within the detector curves charged particle tracks, allowing for momentum measurement. After identification, the four-momenta of each particle are reconstructed. The invariant mass of a candidate decay is computed using:

$$m = \sqrt{(\sum_i E_i)^2 - (\sum_i \vec{p_i})^2} \tag{2.3}$$

where E_i and $\vec{p_i}$ are the energy and momentum of each detected particle [9]. Mass data from candidate decays are binned into histograms, allowing us to perform analysis on the distributions.

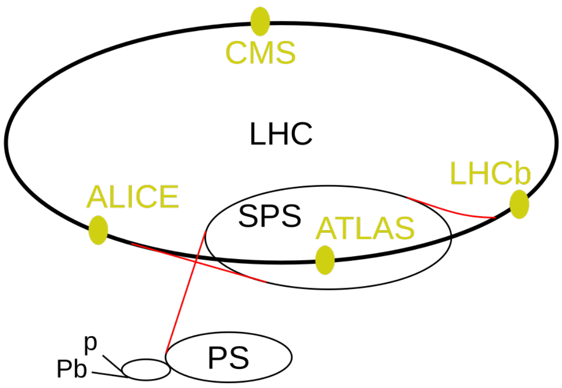

Figure 2.2: The 4 main detectors located at the LHC.

After the signals are recorded by the subsystems, particle trajectories are reconstructed, and a mass hypothesis is assigned to each particle candidate. The particle candidates assigned masses of μ^+ and μ^- are used to reconstruct the invariant mass of the J/ψ particle if they appear to come from a common vertex. The particle candidates assigned masses of K^+ and K^- are used to reconstruct the invariant mass of the ϕ if they appear to come from a common vertex. Applying a common selection framework helps identify misreconstructions between the ϕ and K^{*0} resonances that may arise from particle misidentification in the detector simulation. All pairs of oppositely charged tracks that have $p_{\mathrm{T}} > 1$ GeV and are not identified as muons or electrons are used to reconstruct candidates for the $\phi \rightarrow K^+K^-$. For the $\phi \rightarrow K^+K^-$ candidate, the invariant mass of the track pairs falls within the interval 1008.5 MeV < m(K^-K^+) < 1030.5 MeV. B_s^0 candidates are collected within the mass range 5150-5650 MeV. J/ψ and ϕ tracks are combined to reconstruct the B_s^0 invariant mass distribution. My goal is to examine this invariant mass and determine whether it corresponds to the B_s^0 signal or background.

Chapter 3

Advanced mass model of the B_s^0 meson

3.1 Motivation behind creation of an advanced mass model

CP violation is observed through the cross sections of certain decay channels including that of the $B_s^0 \to J/\psi\phi$ [10]. A direct decay of a B_s^0 to J/ψ is shown in Figure 3.1. The B_s^0 meson can oscillate to the $\bar{B}_s^0$ and vice versa; this is known as $B_s^0 - \bar{B}_s^0$ mixing. This process can be described using a box diagram as seen in Figure 3.2.

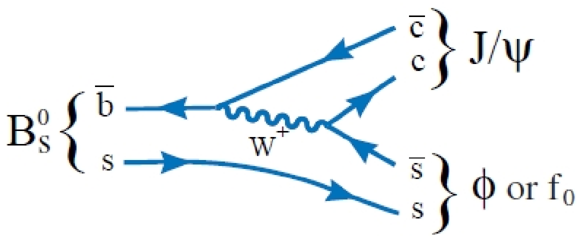

Figure 3.1: Direct decay of $B_s \to J/\psi\phi$.

In the $B_s^0 \to J/\psi\phi$ decay, CP violation arises from the interference between the B_s^0 direct decay and the decay involving $B_s^0 - \overline{B_s^0}$ mixing. Both the B_s^0 and $\overline{B_s^0}$ can decay into $J/\psi\phi$ particles, and their mixing is governed by the mass difference between the heavy (B_H) and light (B_L) mass eigenstates, leading to interference.

The decay amplitudes A_f can be extracted using terms from Eq. (3.1),

$$A_f = (V_{cb}^* V_{cs}) t_f + \sum_{q=u,c,t} (V_{qb}^* V_{qs}) p_f^q \,. \tag{3.1}$$

The t_f describes the amplitude of the tree level diagram and the p_f^q are the amplitudes of the penguin diagrams (seen in Figure 3.3). The dominant contribution to the $B_s^0 \to J/\psi\phi$ comes from the tree-level diagram. This involves a direct $b \to c\bar{c}s$ transition that is mediated by the weak interaction. The penguin amplitudes are smaller.

The phase δ_{13} within the CKM matrix is not directly measured; however, improvement of the B_s^0 mass model refines event selections in distributions which include information about the phase. These include distributions of pseudo-proper lifetime and transverse angular distributions. Pseudo-proper lifetime t distributions probe the lifetime of the particle from the lab-frame perspective according to:

$$t = \frac{m_B L_{xy}}{p_{\mathrm{T}_B}}, \tag{3.2}$$

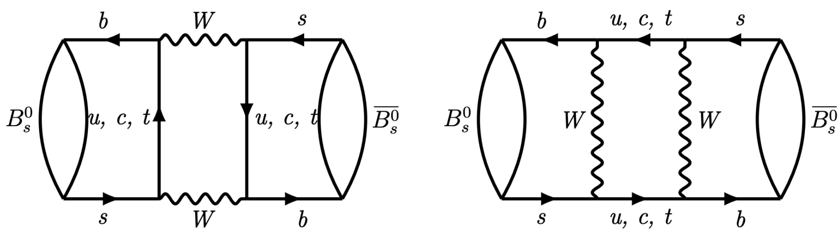

Figure 3.2: Two box diagrams showing the $B_s^0 - \bar{B}_s^0$ oscillation.

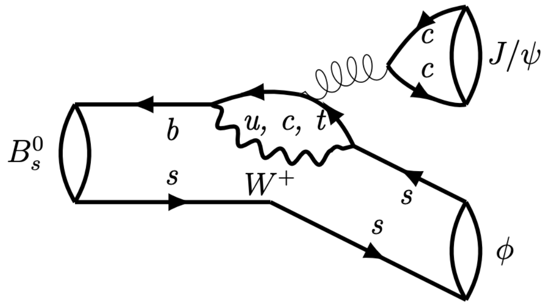

Figure 3.3: The Feynman diagram describing the $B_s^0 \to J/\psi\phi$ decay through a penguin process.

where m_B is the mass of the B_s^0 meson and p_{T_B} is the reconstructed transverse momentum of the B_s^0 candidate. The transverse decay length L_{xy} is the displacement of the B_s^0 meson decay vertex relative to the primary vertex, projected onto the transverse plane (seen in Figure 3.4). The heavy and light mass eigenstates of the B_s^0 meson have associated widths Γ_H and Γ_L which are extracted using pseudo-proper lifetime measurements. The difference between these widths $\Delta\Gamma_s$ can be used to test theoretical predictions with regards to CP violation in the $B_s^0 \to J/\psi\phi$ decay channel. Similarly, effects in mixing-induced CP violation manifest as asymmetries in the transversity angles. Transversity angles describe the orientation of particle spin and momentum in relation to the transverse plane [11]. Such distributions are identified through various kinematic reconstructions, like mass. For more information on the large scale impacts of pseudo-proper lifetime and transverse angular distributions, please see [1]. These distributions can be used to obtain a more accurate value of the characteristic CP-violating phase ϕ_s in the $B_s^0 \to J/\psi\phi$ decay channel. The phase ϕ_s arises from the interference between the direct decay and the decay after $B_s^0 - \bar{B}_s^0$ mixing as defined by

$$\phi_s = -2\arg\left(\frac{V_{ts}V_{tb}^*}{V_{cs}V_{cb}^*}\right) = (-0.0366 \pm 0.0020)\,\mathrm{rad}. \tag{3.3}$$

Here arg refers to the angle that the complex number makes with the positive real axis in the complex plane and the V_{ij} are elements of the CKM matrix seen in Eq. 2.1. Any significant deviation from this measured value would be on indication of New Physics within the B_s^0 system [10].

3.1.1 Signal Plots

This analysis began by using various functions to try to fit a pure B_s^0 signal plot. The signal plot was generated using Monte Carlo data simulating ATLAS data collected during the years

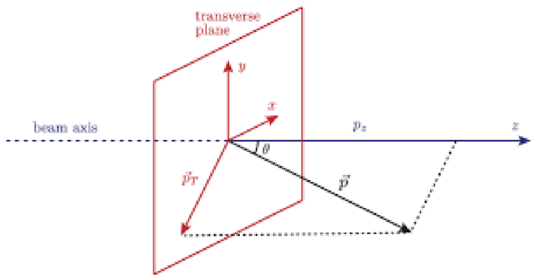

Figure 3.4: A visualization of the transverse plane inside of a collider. The transverse plane is the plane perpendicular to the beam axis. The beam axis is the direction in which a proton beam travels [11].

2015 and 2016. This allowed for fitting without the risk of a function not converging due to any background processes. Some functions were discarded due to shapes inconsistent with the signal. The Johnson-SU [12] and Breit–Wigner [13] distributions were not used to fit the signal as they were deemed inconsistent with the data.

The best function to fit to the signal plot turned out to be a combination of a triple Gaussian and a Crystal Ball distribution. This function fit the data with a χ^2/N_{dof} of 2.69 as seen in Figure 3.5.

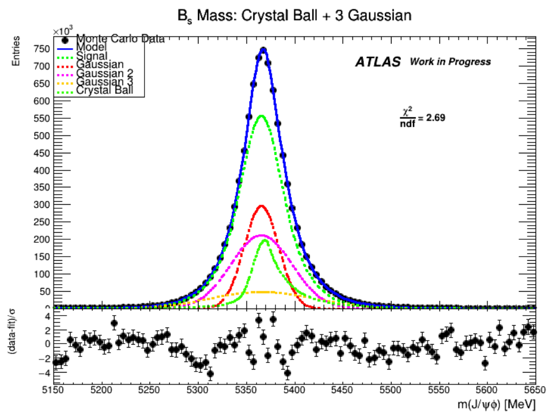

Figure 3.5: Monte Carlo signal events of the $B_s^0 \to J/\psi(\mu^+\mu^-)\phi(K^+K^-)$ channel fitted with Gaussian and Crystal Ball distributions.

3.1.2 Peaking backgrounds

To produce a precise fit of the mass of the B_s^0 meson, the B_s^0 signal must be distinguished from peaking backgrounds. Peaking backgrounds are decays that reconstruct masses consistent with that of the B_s^0.

Resonances that decay via similar final states can lead to misinterpretations by the trigger system. Overlaps in mass between different particles can cause the trigger to incorrectly select such events as part of the signal.

Prominent peaking background decays that contribute to the $B_s^0 \to J/\psi\phi$ decay channel include $B_d^0 \to J/\psi K^{0*}$, $B_d^0 \to \pi^- K^+$ and $\Lambda_s^0 \to J/\psi K^0 p^+$. In this paper, the B_d^0 reconstructions are explored using data collected from LHC Run 2.

3.1.3 $B_d^0 \to J/\psi K^{0*}$ peaking background distribution

The $B_d^0 \to J/\psi K^{0*}$ data are modeled with Monte Carlo data representing ATLAS data from 2015-2016. The generated B_d^0 Monte Carlo samples are used to understand cases where B_d^0 decays are misreconstructed as $B_s^0 \to J/\psi\phi$ candidates when a pion from the $K^{0*} \to K^+\pi^-$ decay is misidentified as a kaon, causing the $K^+\pi^-$ state to mimic a $\phi \to K^+K^-$ decay. When that happens, the event's mass lies within the B_s^0 mass window rather than the usual B_d^0 mass range [1]. After applying the kinematic cuts, a large discrepancy in the shape of the MC B_d^0 mass distribution was noticed.

The reconstructed B_d^0 candidate mass is shown in Figure 3.6 (left). The previous B_s^0 analysis on this channel [1] has a distribution (Figure 3.6 (right)) that looks different from the left image shown in Figure 3.6. The reasons behind the differences in shapes in Figure 3.6 are yet to be discovered. A different file was used for the making of the mass distributions; however the same kinematic cuts were applied.

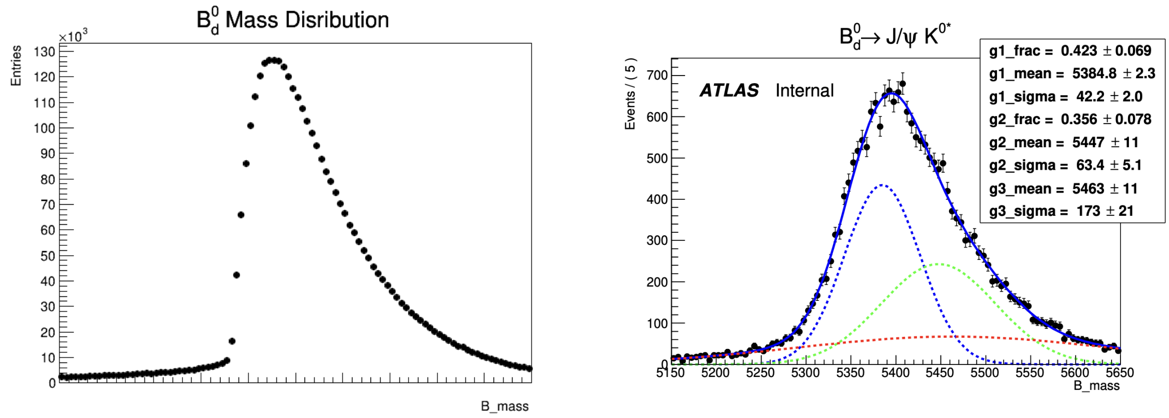

Figure 3.6: The image on the left shows the raw $B_d^0 \to J/\psi K^{0*}$ distribution used for this analysis. The image on the right is the distribution that was used in the previous ATLAS $B_s^0 \to J/\psi\phi$ analysis [1].

Additional two-dimensional plots shown in Figure 3.7 were made to compare the B_d^0 mass to other mass combinations. Exploring the B_d^0 mass versus $K\pi$ mass is important because the most common decay channel for the B_d^0 meson is the $B_d^0 \to J/\psi K^{*0}(\to J/\psi K^-\pi^+)$ decay channel. In the two-dimensional distributions seen in Figure 3.7, we anticipate to see a concentration of events around $m(K\pi) \sim 892$ MeV [14] and $m(B_s^0) \sim 5366$ MeV [15] which are the established mass values for each respective particle. Instead we get a concentration of events in an area that does not match the anticipated $K\pi$ mass values. Comparing the K^-K^+ mass in B_d^0 decays to the $\phi(K^-K^+)$ resonance in the $B_s^0 \to J/\psi\phi$ decay helps identify background contributions. We should again see a concentration of events near $m(B_d^0) \sim 5366$ MeV and $m(\phi) \sim 1020$ MeV but instead we see a nearly uniform distribution of events. Thus the plots seen in Figure 3.7 serve as a validation of incorrect reconstruction in the B_d^0 Monte Carlo samples.

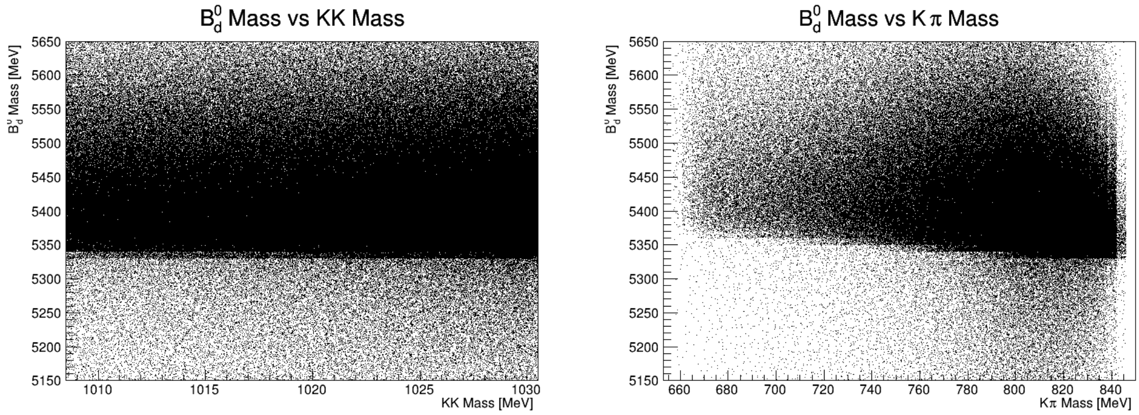

Figure 3.7: The distribution on the left compares the K^-K^+ mass to the mass of the B_d^0 meson in signal MC for the channel $B_d^0 \rightarrow J/\psi K^{*0}$. The distribution of the right compares the $K\pi$ mass to the mass of the B_d^0 meson. These plots were made in an attempt to understand the differences in shapes between the two figures shown in Figure 3.6.

The analysis moved forward with the distribution from the Monte Carlo sample. A triple Crystal Ball fit [16] was able to obtain a $\frac{\chi^2}{Ndof}$ of 8.84 as seen in Figure 3.8. The fitting parameters for the figure were used later in the main mass model to account for the $B_d^0 \rightarrow J/\psi K^{0*}$ peaking background.

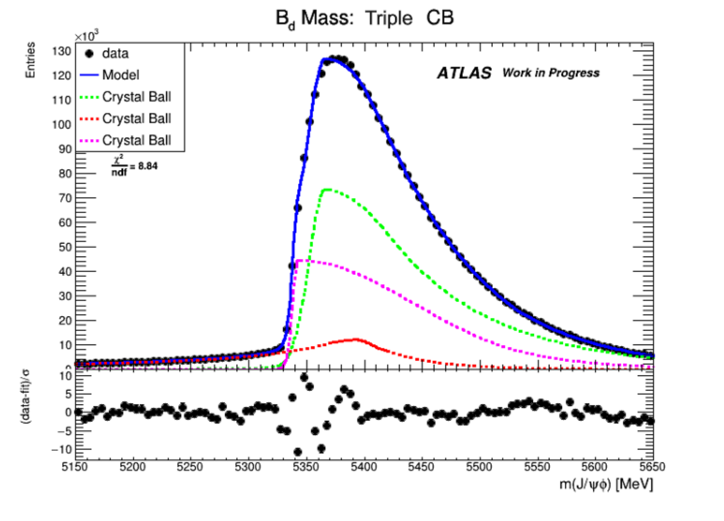

Figure 3.8: $B_d^0 \rightarrow J/\psi K^{0*}$ fit using a triple Crystal Ball function.

3.1.4 Combinatorial backgrounds

Combinatorial backgrounds arise from reconstructed particles with independent decay chains. They are randomly combined to mimic the B_s^0 signal. This is a random, uncorrelated background. Given that the energy of the muons and kaons is uncorrelated, this results in an approximately flat background profile.

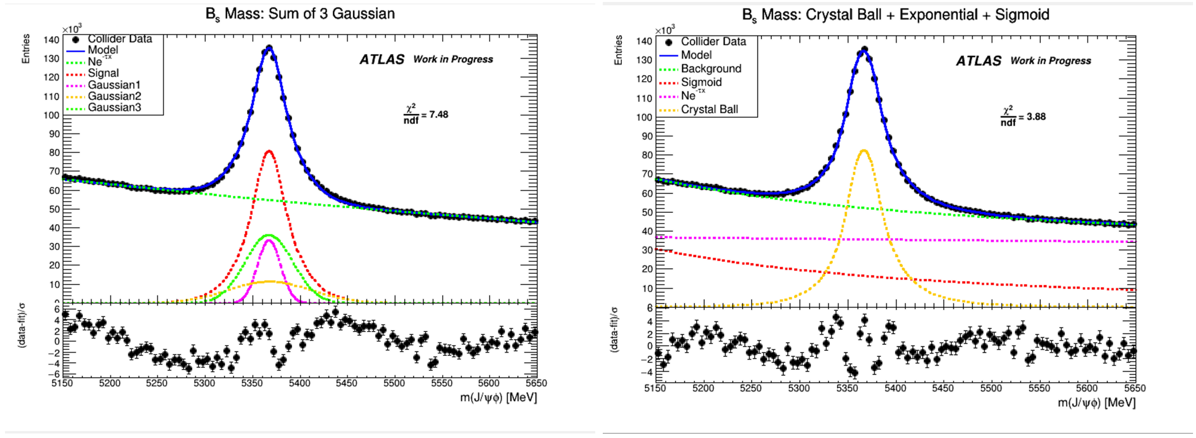

Figure 3.9: Both distributions demonstrate a $B_s^0 \to J/\psi\phi$ mass fit using alternative functions. On the left, a sum of triple Gaussian and an exponential function was used to fit the data. The distribution on the right used a Crystal Ball function to fit the signal and an exponential plus a sigmoid to model the combinatorial background.

3.2 Unique functions

Figure 3.9 shows collision data collected during the years 2015-2018. The mass distribution was reconstructed using particle tracks observed in the ATLAS detector. The particles were identified using the invariant mass of the decay products $J/\psi(\mu^-\mu^+)$ and $\phi(K^-K^+)$, with additional selection criteria based on transverse momentum, pseudorapidity, and detector-specific triggers. Data in Figure 3.9 were fitted using functions to model the $B_s^0 \to J/\psi\phi$ mass distribution including signal and backgrounds. These included the Johnson SU [12], double-sided Crystal Ball [16], and Gaussian distributions.

Figure 3.9 only includes the $B_d^0 \to J/\psi K^{0*}$ peaking backgrounds. The $\Lambda_b^0 \to J/\psi K^0 p^+$ peaking background is not included in Figure 3.9.

The combinatorial backgrounds were fit using exponential functions, sigmoid functions [17] or a combination of the two. Both regular and Chebychev polynomials [18] were not able to converge. First-order to 6th order polynomials were attempted to try to resolve this issue, however the attempts proved unsuccessful.

A mass value for the B_s^0 meson was extracted using the best fits in Figure 3.9. The fitted mass value of the left side of Figure 3.9 is 5366.7 ± 0.1 MeV while the plot on the right gives a value of 5366.8 ± 0.3 MeV, which is consistent with the established value of $m_{B_s^0} = 5366.93 \pm 0.10$ MeV [15].

3.3 Results for different Run 2 years

B_s^0 mass reconstruction was carried out separately for each of the different ATLAS Run 2 years. This was done to ensure that ATLAS reconstructs a consistent mass peak year by year as any deviation from this anticipated result could be a sign of detector miscalibration. Years 2015, early 2016, late 2016, 2017, and 2018 data were all analyzed separately.

These distributions too were plotted with a variety of alternative functions. The alternative function used for each fit varies year by year. The functions include Gaussians, Crystal Ball, and Johnson-SU distributions. The best results for each year are shown in Figure 3.10. The $\frac{\chi^2}{N_{dof}}$ values span from 0.89 to 1.21. The most successful fitted distributions are a sum of 3 Gaussian distributions and an exponential plus a sigmoid function to fit the combinatorial backgrounds.

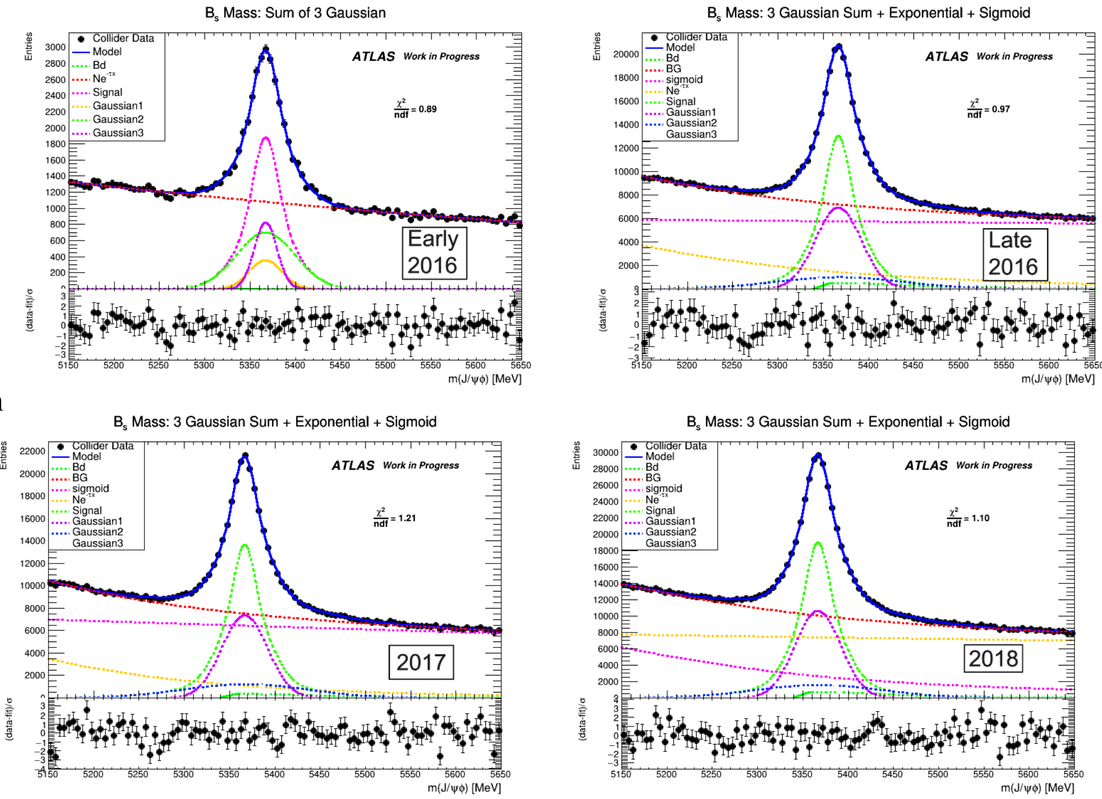

hh

Figure 3.10: B_s^0 fitted mass distributions from years 2015-2018.

The peak mass values shown in Table 3.1 for each individual LHC Run 2 year are consistent with the established value of $m_{B_s^0} = 5366.93 \pm 0.10$ MeV.

Run 2 Year	Fitted peak mass (MeV)	χ^2/N_{dof}
2015	5367.3 ± 0.3 (stat.) $\pm$ 0.6 (syst.)	1.01
Early 2016	5367.3 ± 0.3 (stat.) $\pm$ 0.6 (syst.)	0.89
Late 2016	5367.3 ± 0.3 (stat.) $\pm$ 0.6 (syst.)	0.97
2017	5366.7 ± 0.1 (stat.) $\pm$ 0.1 (syst.)	1.21
2018	5366.7 ± 0.1 (stat.) $\pm$ 0 (syst.)	1.10

Table 3.1: The fitted peak values for different LHC Run 2 data selection years.

The systematic errors given in Table 3.1 were calculated as the difference between the model used in this work and the maximum likelihood fitting model as described in Table 3.2 and its caption.

The results for all the years in Table 3.1 are consistent within one σ of combined statistical and systematic error.

3.4 Results for different p_{T} regions

The images in Figure 3.11 report the reconstructed B_s^0 mass for different ranges of B_s^0 p_{T}. The p_{T} regions are 10-20, 20-40, and 40-150 GeV. The higher p_{T} ranges may reveal effects of New Physics, like heavy resonance production.

Run 2 Year	ML fit (MeV)
2015 / 2016	5366.8 $\pm$ 0.1 (stat.)
2017	5366.6 $\pm$ 0.1 (stat.)
2018	5366.7 $\pm$ 0.1 (stat.)

Table 3.2: The fitted mass peak using a maximum likelihood (ML) fit with per candidate invariant mass errors measured directly from the tracking of each event, used in previous B_s^0 publication [1].

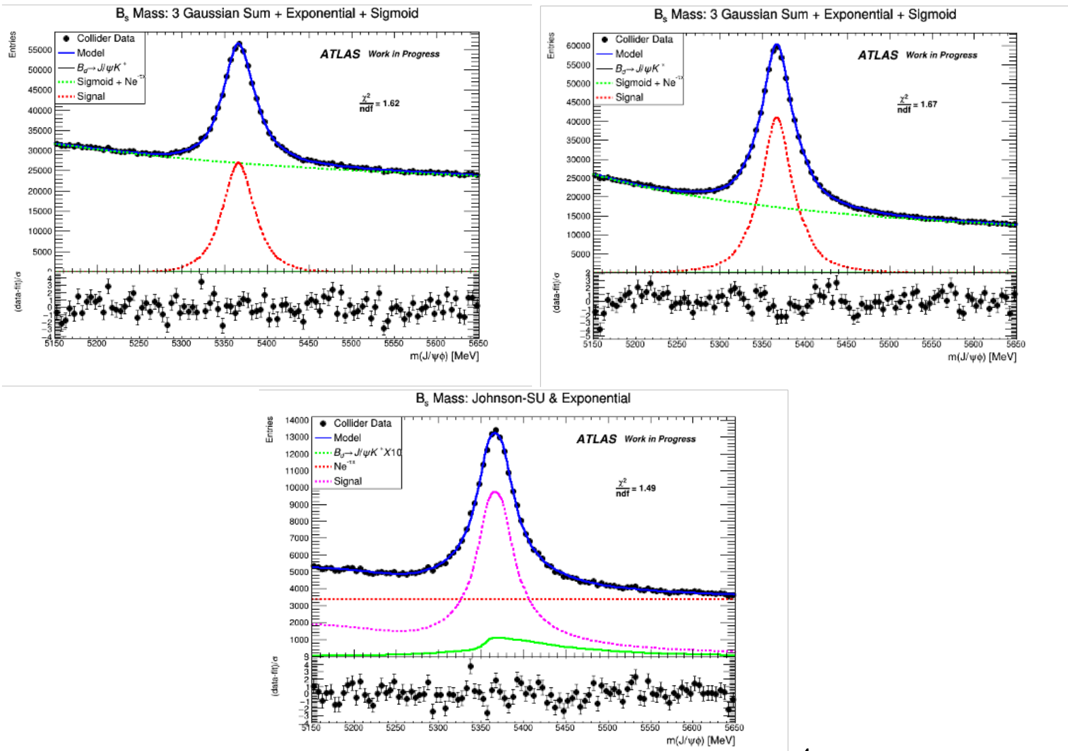

4

Figure 3.11: The $B_s^0 \to J/\psi\phi$ mass distribution for B_s^0 p_{T} in different transverse momentum regions. (Left) The fitted mass distribution for the p_{T} region of 10-20 GeV. (Middle) The fitted mass distribution for the p_{T} region of 20-40 GeV. (Right) The fitted mass distribution for the p_{T} region of 40-150 GeV.

p_{T} region (GeV)	Fitted B_s^0 peak mass (MeV)	χ^2/N_{dof}
10-20	5366.4 $\pm$ 0.1	1.62
20-40	5366.7 $\pm$ 0.1	1.67
40-150	5366.4 $\pm$ 0.2	1.49

Table 3.3: The fitted B_s^0 mass peak values for different p_{T} regions.

Table 3.3 shows a χ^2/N_{dof} of 1.62, 1.67, and 1.49 for the 10-20, 20-40, and 40-150 GeV p_{T} regions respectively. The best fitting function for the 10-20 and 20-40 GeV p_{T} regions is a sum of 3 Gaussians plus an exponential and a sigmoid function, while the 40-150 GeV p_{T} region was fitted using a sum of triple SU-Johnson function plus an exponential function, as seen in Figure 3.11. The fitted mass peaks for all three p_{T} regimes lie within 0.01 % absolute error with respect to the established value of 5366.9 ± 0.2 MeV [15].

Chapter 4

Conclusion

This study presents an approach to the modeling of the $B_s^0 \rightarrow J/\psi\phi$ mass distribution. By using alternative functions to fit the B_s^0 mass distribution, we have sought to improve the precision of parameters used to characterize the CP-violating phase angle within $B_s^0 - \overline{B_s^0}$ mixing. The stability of the mass distribution across different Run 2 datasets and transverse momentum (p_{T}) regions was also assessed. A mass of 5366.7 $\pm$ 0.1 MeV for the B_s^0 was observed. The distribution was found to vary within systematic uncertainties for relevant p_{T} and time regimes. The study aided in determining a more accurate CP-violating phase angle by reducing potential selection year and transverse momentum region biases from mass modeling.

References

[1] ATLAS Collaboration. "Measurement of the CP-violating phase ϕ_s in $B_s^0 \to J/\psi\phi$ decays in ATLAS at 13 TeV." In: *CERN* (2020). cds.cern.ch/record/2703988/ATL-COM-PHYS-2019-1454.pdf.

[2] https://en.wikipedia.org/wiki/Monte_Carlo_method.

[3] *Standard Model of Particle Physics*. 2025. https://en.wikipedia.org/wiki/Standard_Model.

[4] *What is the Universe made of?* https://www.esa.int/Science_Exploration/Space_Science/Extreme_space/What_is_the_Universe_made_of. European Space Agency, [Accessed 2025-01-02].

[5] https://home.cern/science/physics/matter-antimatter-asymmetry-problem.

[6] Alexander Lenz and Ulrich Nierste. "Theoretical update of $B_s - \bar{B}_s$ mixing." In: *Journal of High Energy Physics* 2007.06 (June 2007), pp. 072–072. ISSN: 1029-8479. DOI: 10.1088/1126-6708/2007/06/072. http://dx.doi.org/10.1088/1126-6708/2007/06/072.

[7] A. D. Sakharov. "Violation of CP Invariance, C asymmetry, and baryon asymmetry of the universe." In: *Pisma Zh. Eksp. Teor. Fiz.* 5 (1967), pp. 32–35. DOI: 10.1070/PU1991v034-05ABEH002497.

[8] ATLAS Collaboration. "The ATLAS experiment at the Large Hadron Collider," in: *JINST* 3 (2008), S08003.

[9] Martin Zeman. "Measurement of the Standard Model WW production cross-section using the ATLAS experiment on the LHC." NNT: 2014PA112263. Ph.D. dissertation. Université Paris Sud - Paris XI, 2014. https://cds.cern.ch/record/2012593/files/Thesis-2014-Zeman.pdf.

[10] Radek Novotny. "Study of b-quark Processes Using the ATLAS Detector". Ph.D. dissertation. Czech Technical University, 2020. https://cds.cern.ch/record/2741578/files/CERN-THESIS-2020-145.pdf.

[11] Roberto Franceschini et al. *Kinematic Variables and Feature Engineering for Particle Phenomenology*. 2022. arXiv: 2206.13431 [hep-ph]. https://arxiv.org/abs/2206.13431.

[12] https://variation.com/wp-content/distribution_analyzer_help/hs126.htm.

[13] https://en.wikipedia.org/wiki/Relativistic_Breit%E2%80%93Wigner_distribution.

[14] https://pdg.lbl.gov/2014/tables/rpp2014-tab-mesons-strange.pdf.

[15] https://pdg.lbl.gov/2024/tables/contents_tables_mesons.html.

[16] Dmitry A Romanov. *Crystal ball function*. https://www.jlab.org/primex/weekly_meetings/slides_2009_07_17/dmitry/crystalball.html.

[17] https://www.geeksforgeeks.org/derivative-of-the-sigmoid-function/#.

[18] https://mathworld.wolfram.com/ChebyshevPolynomialoftheFirstKind.html.